

KA-TP-21-2021
TTP21-035
CERN-TH-2021-153
P3H-21-070
ZU-TH 48/21
IPPP/21/39

Top-quark mass effects in H +jet and H +2 jets production

X. Chen,^{1,2,3} A. Huss,⁴ S. P. Jones,⁵ M. Kerner,^{1,2,3} J.-N. Lang,³ J. M. Lindert,⁶ H. Zhang^{3,7}

¹*Institute for Theoretical Physics, Karlsruhe Institute of Technology, 76131 Karlsruhe, Germany*

²*Institute for Astroparticle Physics, Karlsruhe Institute of Technology, 76344 Eggenstein-Leopoldshafen, Germany*

³*Physik-Institut, Universität Zürich, CH-8057 Zürich, Switzerland*

⁴*Theoretical Physics Department, CERN, 1211 Geneva 23, Switzerland*

⁵*Institute for Particle Physics Phenomenology, Durham University, Durham, DH1 3LE, UK*

⁶*Department of Physics and Astronomy, University of Sussex, Brighton BN1 9QH, UK*

⁷*Institut für Theoretische Teilchenphysik, Karlsruhe Institute of Technology, 76128 Karlsruhe, Germany*

ABSTRACT: We present calculations of Higgs boson production via gluon-gluon fusion in association with one or two additional jets at next-to-leading order in QCD. The calculation of H +jet is exact in the treatment of the top-quark mass, whereas for the H +2 jets calculation the two-loop virtual amplitudes are approximated via a reweighting with leading-order mass effects, while keeping all top-quark mass effects in the real radiation contributions. For H +jet production, this study extends a previous calculation, revealing an error in the previous results. For total and differential cross sections, we present new results and compare the QCD corrections with the infinite top-mass limit, for which we find a strikingly good agreement if all amplitudes are rescaled by the leading-order mass dependence.

Contents

1	Introduction	1
2	Analysis framework and tools	3
2.1	Parton level event generator: NNLOJET	4
2.2	One-loop contributions: OPENLOOPS2.2	4
2.3	Two-loop contributions: SECDEC-3	6
3	Numerical results	6
3.1	Setup	6
3.2	Fiducial total cross sections	7
3.3	Fiducial differential cross sections for H+jet production	8
3.4	Fiducial differential cross sections for H + 2 jets production	10
4	Conclusions	12
A	Inclusive cross sections	13

1 Introduction

The current and upcoming runs of the Large Hadron Collider (LHC) are stress-testing the Standard Model (SM) of particle physics at an unprecedented level. In this respect one of the main objectives of Run 3 and the high-luminosity phase of the LHC (HL-LHC) will be a further detailed investigation of the Higgs sector. The abundant future data samples will allow the range of Higgs analyses to be extended to multi-dimensional measurements and high-energy tails of kinematic distributions. A key observable in this regard is the transverse momentum distribution of the Higgs boson, $p_{T,H}$, which serves as a unique probe of physics Beyond the Standard Model (BSM) [1–10]. Given the expected experimental data sets, this distribution will be measured both inclusively and in association with jets up to several hundreds of GeV in the Higgs transverse momentum [11, 12]. Already now experimental measurements by ATLAS and CMS yield sensitivity up to few hundred GeV [13, 14].

Both in the inclusive case and for the production in association with jets, the dominant Higgs production mode in the SM originates via a top-quark loop in gluon-gluon fusion, however, at large transverse momentum eventually also vector-boson fusion (VBF), Higgsstrahlung (VH) and top-pair associated Higgs production contribute significantly [15]. For the production in association with jets, additional constraints on jet invariant masses and/or rapidities allow the relative fraction of the VBF events to be enhanced [16, 17]. Precise VBF measurements will allow us to constrain on the one hand the electroweak (EW) couplings of the Higgs, and on the other hand when restricting to large Higgs transverse momentum they will allow for complementary constraints on models of new physics [18–23]. In this regard, one of the dominant uncertainties in VBF measurements originates from the background modelling of the gluon-induced Higgs production mode.

The loop-induced nature of the gluon-gluon fusion Higgs production process makes higher-order corrections notoriously difficult to calculate. In QCD fixed-order perturbation theory including mass effects, inclusive Higgs production at next-to-next-to-leading order (NNLO) was calculated only very recently [24], Higgs plus jet production is known at next-to-leading order (NLO) [25–28], while Higgs plus dijet production (and beyond) is only known at leading order (LO) [29–33]. In the

NLO computations of Higgs plus jet production the crucial two-loop virtual contributions have been obtained numerically [34, 35] in Refs. [25, 28] respectively via a suitable high-energy expansion [36] in Refs. [26, 27].

Formally, below the top-quark threshold, higher precision can be achieved via the heavy top loop (HTL) approximation, effectively integrating out the top-quark loop [37]. In the HTL approximation, inclusive Higgs production is known at N3LO [38–42], Higgs plus jet production at NNLO [43–47], and Higgs plus dijet production at NLO [48, 49] (for Higgs plus trijet production see [50]). For inclusive Higgs production and for $p_{T,H} < m_t$ (where m_t is the top-quark mass) predictions in the full SM and in the HTL agree at the percent level. For $p_{T,H} \ll m_t$ eventually fixed-order perturbation theory becomes unreliable and a matching to higher logarithmic accuracy becomes mandatory [51–57], and also bottom-quark effects have to be considered [58–64].

At the other end of the spectrum, for $p_{T,H} > m_t$, the accuracy of the HTL quickly deteriorates due to a different high-energy scaling compared to the full theory [65]. For $p_{T,H} = 500(1000)$ GeV the two differ by a factor of about 4(10). In this high-energy regime in order to improve with respect to the HTL additional $\mathcal{O}(1/m_t)$ corrections have been investigated [31, 66, 67]. Overall, the above cited explicit fixed-order computations have shown that higher-order corrections computed in the HTL rescaled with lower-order predictions with explicit mass dependence yield remarkably good approximations of the full result despite the fact that the HTL is not valid in this energy regime. Therefore, it appears to be justified to tentatively apply this very same procedure also at the highest perturbative orders, where validation of the approximation is not yet possible. An example of such an approximation at the currently highest available perturbative order is presented in Ref. [15] for Higgs plus jet production where NNLO corrections in the HTL are combined with NLO corrections in the full SM. However, defining a reliable uncertainty on such approximations remains crucial. Such approximations of reweighting higher-order computations in the HTL with exact lower order results are also at the basis of all currently available NLO Monte Carlo predictions matched to parton showers for Higgs plus (multi-)jet production [68–72].

In this paper we present fixed-order NLO QCD computations for $pp \rightarrow H + j$ and also $pp \rightarrow H + jj$ including top-quark mass effects. The computation for $pp \rightarrow H + j$ continues the study of Ref. [25], i.e. two-loop virtual corrections in the full SM are evaluated numerically via SECDEC-3 [34, 35]. Here we present additional kinematic observables besides the $p_{T,H}$ distribution already shown in Ref. [25] and compare the relative higher-order corrections in the full SM against the HTL, and also an alternative approximation known as $\text{FT}_{\text{approx}}$, which has been introduced in Ref. [73] in the context of calculations for multi-Higgs production. In the $\text{FT}_{\text{approx}}$ all ingredients of the NLO computation are computed exactly, except for the two-loop virtual contributions, which are approximated in the HTL and reweighted with LO mass dependence. In the case of $pp \rightarrow H + jj$ production we compare results in the HTL and in the $\text{FT}_{\text{approx}}$, as the exact five-point two-loop virtual amplitudes remain beyond current technology. The main aim of this study is three-fold: firstly, we would like to offer complementary kinematic information for the $pp \rightarrow H + j$ process, while also offering a (partial) validation of the results already presented in Ref. [25]. In this respect, the present study uncovered an issue affecting the real corrections included in Ref. [25], which has subsequently been rectified. Secondly, we would like to investigate the $pp \rightarrow H + jj$ process in a kinematic regime relevant for VBF analyses. The comparison of NLO/LO ratios (usually known as K-factors) among HTL, $\text{FT}_{\text{approx}}$ and the full SM will help to put results obtained in a reweighted HTL on a more solid footing. Thirdly, results presented in this study can be seen as an intermediate step towards an NNLO computation of $pp \rightarrow H + j$ including exact mass effects wherever possible.

Technically, the computations of the NLO corrections to $pp \rightarrow H + j$ and $pp \rightarrow H + jj$ production are performed within the NNLOJET fixed-order Monte Carlo framework, which employs antenna subtraction for the handling of infrared (IR) singularities [74–82]. All loop-squared amplitudes are evaluated via a new interface between NNLOJET and OPENLOOPS2 [83–85] based on the latest

(soon to be released) version OPENLOOPS2.2 which in turn implements a new reduction method called *Otter* [86], which ensures excellent numerical stability in particular of the loop-induced real radiation amplitudes deep into the unresolved regime. We will investigate and discuss this numerical stability issue explicitly.

The structure of the paper is as follows. In Section 2 we describe the computational setup and employed tools. Numerical results for H +jet and H +2 jets production will be presented in Section 3. We will conclude in Section 4.

2 Analysis framework and tools

In this paper, we present predictions for the production of a boosted Higgs boson in the gluon-fusion channel. We consider Higgs bosons produced in association with one ($pp \rightarrow H + j$) or two ($pp \rightarrow H + jj$) jets with NLO QCD corrections and include the effects of a finite top-quark mass either fully or via a suitable approximation. For $pp \rightarrow H + j$ we compute the transverse momentum distribution of the Higgs boson including a finite top-quark mass, which has appeared previously in the literature [25–28], as well as the Higgs boson plus jet invariant mass distribution. For $pp \rightarrow H + jj$, the virtual corrections involve two-loop amplitudes for $2 \rightarrow 3$ scattering. The mathematical complexity of the virtual corrections makes their computation currently intractable using either numerical or analytical methods. We therefore adopt an approximation scheme to the full theory (FT_{approx}) [73, 87] for the NLO QCD corrections to Higgs boson plus two jet production. Specifically, we include the exact top-quark mass dependence (SM) in the real corrections and infrared singular subtraction terms while using the virtual corrections in the heavy top-quark limit (HTL) re-weighted by the full Born level contribution on an event-by-event basis. In fact, although the full matrix elements relevant to the virtual contributions of $H + 2$ jets production are currently not available, nevertheless, their explicit infrared divergence at NLO can be predicted by the Catani dipole structure [88]:

$$\text{Pole}\{|\mathcal{M}_4^2(m_t, \mu_R^2; \{p\})|^2\} = \sum \mathbf{I}^{(1)}(\epsilon, \mu_R^2; \{p\}) |\mathcal{M}_4^1(m_t; \{p\})|^2, \quad (2.1)$$

where m_t is the top-quark mass, μ_R^2 is the renormalisation scale, $\{p\}$ is the momentum set regarding all external particles, $|\mathcal{M}_n^m|^2$ is the matrix element with n legs and m loops and $\mathbf{I}^{(1)}(\epsilon, \mu_R^2; \{p\})$ is the dipole operator containing all explicit IR divergences in d space-time dimensions. The explicit expressions for dipole operators at squared matrix element level can be found in [74]. We estimate the finite contribution of $|\mathcal{M}_4^2(m_t, \mu_R^2; \{p\})|^2$ by re-weighting the corresponding matrix element in the HTL approximation ($m_t \rightarrow \infty$) using:

$$|\mathcal{M}_4^2(m_t, \mu_R^2; \{p\})|^2 \rightarrow |\mathcal{M}_4^1(\infty, \mu_R^2; \{p\})|^2 \frac{|\mathcal{M}_4^1(m_t; \{p\})|^2}{|\mathcal{M}_4^0(\infty; \{p\})|^2}. \quad (2.2)$$

Consequently, Eq.(2.2) also recovers the explicit pole structure in Eq.(2.1) and the explicit pole cancellation in the second bracket of Eq.(2.3) is automatically retained.

The FT_{approx} scheme has proved to be remarkably reliable for Higgs plus one jet [47] production and, to a lesser extent, di-Higgs [89] production (however in the latter case, it is much less reliable for differential distributions) at the LHC. We implement and present the first application of this approximation to Higgs boson plus two jet production at NLO in QCD.

In the following sections we document the detailed implementation of our calculations. The NNLOJET program is used as a parton level event generator and all Born and real radiation one-loop contributions are computed using OPENLOOPS2.2. The two-loop matrix elements involving a finite top-quark mass for $pp \rightarrow H + j$ are computed exactly using SECDEC-3.

2.1 Parton level event generator: NNLOJET

NNLOJET is a parton-level event generator equipped with flexible histogram analysis tools and scattering matrix elements evaluated in both the HTL approximation and in the full SM. It implements the antenna subtraction method to cancel infrared singularities from higher order QCD corrections [74–82] while retaining the fully differential information of final state particles.

In this study, we combine NNLOJET with loop induced matrix elements provided by OPENLOOPS2 and SECDEC-3 to study finite top-quark mass corrections for H+jet and H + 2 jets production with NLO QCD corrections. The HTL and SM have the same infrared singular behaviour for both real emissions and virtual corrections, the antenna subtraction method can therefore be readily applied to regulate infrared singularities at NLO for loop-induced processes. Schematically, the fully differential NLO contribution takes the form:

$$\begin{aligned} d\sigma_{H+n\text{jet}}^{\text{NLO}} = & \int_{d\Phi_{n+1}^H} \left[|\mathcal{M}_{n+3}^1(m_t; \{p\})|^2 - \sum_{\{p\}} X_3^0 |\mathcal{M}_{n+2}^1(m_t; \{\tilde{p}\})|^2 \right] \\ & + \int_{d\Phi_n^H} \left[|\mathcal{M}_{n+2}^2(m_t, \mu_R^2; \{p\})|^2 + \sum_{\{p\}} \mathcal{X}_3^0 |\mathcal{M}_{n+2}^1(m_t; \{p\})|^2 \right], \end{aligned} \quad (2.3)$$

where Φ_n^H is the final state phase space of one Higgs plus n partons, X_3^0 represents the tree-level three-parton antenna functions, \mathcal{X}_3^0 represents the corresponding integrated antenna functions in d -dimensions and $\{\tilde{p}\}$ is the momentum set after antenna mapping with one less parton compared to the $\{p\}$ momentum set. We use X_3^0 and the corresponding reduced matrix elements ($|\mathcal{M}_{n+2}^1|^2$) to capture the infrared singular behaviour of real radiations in $|\mathcal{M}_{n+3}^1|^2$, leading to a infrared finite contribution of the first bracket in Eq.(2.3). By adding back the integrated antenna functions \mathcal{X}_3^0 in the second bracket of Eq.(2.3), we render the integrand over the Φ_n^H phase space IR finite. The explicit IR divergences (which appear as poles in the regulator ϵ) cancel analytically with the explicit IR poles from the virtual contribution ($|\mathcal{M}_{n+2}^2|^2$).

2.2 One-loop contributions: OPENLOOPS2.2

All one-loop amplitudes contributing at the Born and real radiation level are provided by the OPENLOOPS2.2 package, an upcoming improved version of the OPENLOOPS2 program which implements a new reduction method called *Otter* [86]. Compared to the original algorithm [83], OPENLOOPS2 includes significant improvements in numerical stability and performance for the computation of tree-loop interference amplitudes. These improvements were achieved by a combination of the so-called on-the-fly reduction algorithm [84] and an automated stability system. However, the current implementation, which was designed for tree-loop interferences, cannot be directly applied to loop-induced amplitudes, such as those required for the present computation. In OPENLOOPS2.2 a new tensor integral reduction method has been developed, based on the on-the-fly reduction algorithm [84], that can also be used for loop-squared amplitudes. It profits from recent improvements in performance and methods developed for handling numerical instabilities. More specifically, numerical instabilities are avoided by using certain freedoms in the selection of the reduction identities, and analytical any-order expansions of three-point tensor integrals in the limit of small Gram determinant [85]. Furthermore, within OPENLOOPS2.2 residual instabilities are captured by a rescaling test and tensor integrals are recomputed in quadruple precision in case the given accuracy is not reached. This upgrade to quadruple precision is efficient, and also important for computations in deep infrared regions. OPENLOOPS2.2 depends on COLLIER [90] only for double precision scalar integrals and on ONELOOP [91] for quadruple precision scalar integrals.

Numerical stability The numerical stability of OPENLOOPS2.2 is crucial for the calculations of H+jet and H + 2 jets productions presented in this paper, especially to contributions from infrared

kinematical regions, which are numerically challenging. In Fig. 1 we illustrate as a benchmark the stability of the critical $gg \rightarrow Hgg$ and $gg \rightarrow Hggg$ amplitudes subject to single soft or collinear radiation. The degree of softness and collinearity are defined as

$$\xi_{\text{soft}} = E_{\text{soft}}/\sqrt{s}, \quad \xi_{\text{coll}} = \theta_{ij}^2, \quad (2.4)$$

where E_{soft} is the energy of the soft particle, and θ_{ij} denotes the angle of the collinear branching. The numerical stability is defined as

$$\mathcal{A} = \log_{10} \left(\frac{\mathcal{W} - \mathcal{W}^{(0)}}{\mathcal{W}^{(0)}} \right), \quad (2.5)$$

where \mathcal{W} denotes the one-loop-squared matrix element, $\mathcal{W}^{(0)}$ is the benchmark result, and \mathcal{A} corresponds to the number of stable digits up to a minus sign. As can be seen from these plots, the numerical accuracy remains very high all the way down to the deep infrared regime.

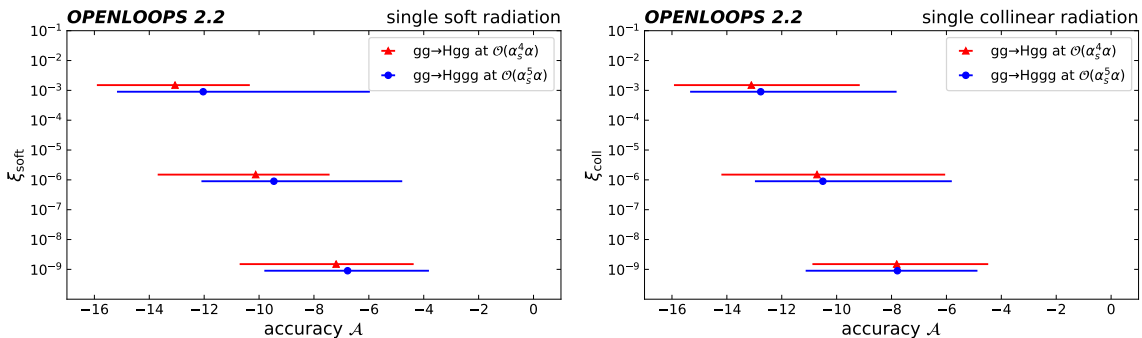


Figure 1: Stability plots in IR regions for one-loop-squared matrix elements in $gg \rightarrow Hgg$ and $gg \rightarrow Hggg$ versus the degree of collinear ξ_{coll} or soft ξ_{soft} singularity obtained with OPENLOOPS2.2. For each value of $\xi_{\text{soft/coll}}$, the numerical accuracy is calculated with a sample of 10^3 randomly distributed infrared events. Unstable points are detected by a rescaling test and rescued if the relative accuracy of 10^{-6} is not reached. The rescue step reevaluates the tensor integrals to quad precision. The accuracy of the so-obtained value is determined by comparing it to a quadruple precision benchmark whose accuracy is also assessed by a rescaling test. The plotted central points and variation bands correspond, respectively, to the average and 100% confidence interval of \mathcal{A} .

Numerical performance In Table 1 we present results for the average evaluation time of samples of random phase-space points using various different modes/versions of OPENLOOPS. In particular, here certain parts of the amplitude are evaluated in double or in quadruple precision, or a realistic error estimate of the amplitudes is performed. In summary, performance is greatly improved in OPENLOOPS2.2 which in particular makes a tensor integral based rescaling test cheap. Moreover, since OPENLOOPS2.2 operates also in quadruple precision with very high numerical efficiency, numerically unstable points can be rescued in a reliable way, which has largely been prohibitive for loop-squared amplitudes in OPENLOOPS2. In fact, OPENLOOPS2.2 allows for rescue of unstable points in a new hybrid mode, where only the tensor integrals are evaluated in higher numerical precision resulting in a 8-fold and 3-fold increase in runtime compared to pure double precision for $gg \rightarrow Hgg$ and $gg \rightarrow Hggg$ respectively, compared to a roughly 80-fold increase in runtime for full quadruple precision. In practice, and as used for the present computation of this paper in OPENLOOPS2.2 a combination of pure double precision with this new hybrid mode is used. Based on a pure double precision evaluation the stability for every phase-space point is estimated based on a rescaling test of only the tensor integrals. Then, only for critical points the tensor integrals are reevaluated in quadruple precision based on the hybrid mode.

Mode	$gg \rightarrow Hgg$ (time/psp)	$gg \rightarrow Hggg$ (time/psp)
OL2.1+Collier DP	13ms	0.56s
OL2.1+Collier DP + error estimation	19ms	0.89s
OL2.1+CutTools QP	43000ms	2300s
OL2.2+Otter DP	8.9ms	0.29s
OL2.2+Otter DP + error estimation	11ms	0.32s
OL2.2+Otter DP+QP tensor integrals	68ms	0.87s
OL2.2+Otter QP	740ms	23s

Table 1: Runtimes for loop-squared amplitudes for $gg \rightarrow Hgg$ and $gg \rightarrow Hggg$ in OPENLOOPS. All numbers have been produced on an Intel(R) Core(TM) i7-7700 CPU @ 3.60GHz. The first three rows correspond to the modes so far available in OPENLOOPS2 [85]. These employ double precision evaluation with COLLIER (first and second row), where in the second row tensor integrals are computed twice using the COLI and DD branches of COLLIER in order to obtain an error estimate. The third row employs CUTTOOLS and the entire amplitude is evaluated in quadruple precision. For the amplitudes at hand the resulting runtimes in quadruple precision are prohibitive to be used as rescue system. The lower four rows represent evaluation based on the new *Otter* method in OPENLOOPS2.2. In this case the error estimation is performed via a rescaling test where all tensor integrals are recomputed with rescaled kinematics. The sixth row corresponds to a new hybrid mode where only the tensor integrals are evaluated in quadruple precision, and everything else in double precision. The last row shows the performance for a full quadruple precision evaluation within OPENLOOPS2.2.

2.3 Two-loop contributions: SECDEC-3

For $pp \rightarrow H + j$ production, we evaluate the two-loop virtual contributions with exact top-quark mass dependence as presented in Refs. [25, 28]. Briefly, the two-loop amplitudes, which depend on four mass scales (the Mandelstam invariants s and t as well as the two masses m_t and m_h), are expressed in terms of a basis of master integrals using the program REDUZE2 [92]. In order to obtain the integral reduction in a reasonable time and to reduce the size of the resulting amplitude, the ratio of the Higgs boson mass to the top-quark mass is fixed according to $m_H^2/m_t^2 = 12/23$. The master integrals are then sector decomposed using the program SECDEC-3 [34, 35] and numerically integrated on Graphics Processing Unit (GPUs) using the Quasi-Monte Carlo method [93, 94]. To improve the stability of the amplitude we select a quasi-finite basis of master integrals as outlined in Ref. [28], this differs from the basis originally used in Ref. [25]. We observe that the new choice of master integrals also significantly reduces the complexity of the coefficients of the master integrals appearing in the amplitude and thus the size of the code.

The results presented here are produced using a total of 6497 phase-space points for the two-loop virtual contribution. In Ref [25], a fraction of the phase-space points were distributed such that they provide a good estimate of the total cross section (assuming a jet cut of $p_{T,j} > 30$ GeV) and additional phase-space points were generated to sample the tail of the $p_{T,H}$ distribution. We reuse these existing phase-space points and also compute an additional 1007 points to populate the large invariant mass region m_{Hj} for $p_{T,j} > 300$ GeV.

3 Numerical results

3.1 Setup

As an extension of the study of Higgs plus one jet production at NLO [25], we adopt the same input parameters and numerical setup in the current calculation. To quantify the impact of increasing

the number of final state jets, we keep the input parameters consistent between H+jet and H + 2jets production. The counting of the number of jets in this study is inclusive. There is no difference between inclusive and exclusive jet counting for LO while results at NLO accuracy receive contributions from real emissions including events classified with one additional jet. For the Higgs and top-quark mass we use $m_H = 125$ GeV and $m_t = 173.055$ GeV. The top-quark Yukawa coupling $\lambda_t = \sqrt{2}m_t/v$ is determined by the vacuum expectation value (vev) of the Higgs $v = \frac{M_W \sin \theta_W}{\sqrt{\pi\alpha_{\text{QED}}}} = 246.219$ GeV and the top-quark mass. We use the five flavour scheme assuming light quarks are massless in both initial and final states.

Throughout our calculation, the top-quark mass is renormalised using the on-shell (or pole mass) scheme. It has been pointed out in the literature that several Higgs boson production processes (including Higgs boson production in association with jets) are sensitive to the scheme and scale used to renormalise quark masses [95–98]. For example, at LO, the difference between the pole mass scheme and the $\overline{\text{MS}}$ scheme at scale $m_{H,j}/2$ was found to be around 12% for $m_{H,j} = 700$ GeV and $p_{T,j} > 300$ GeV. At larger $p_{T,H}$ the difference between the two schemes grows and can reach $\approx 25\%$ for $p_{T,H} = 1$ TeV. In off-shell Higgs boson production, off-shell Higgs boson decay to photons and in Higgs pair production, the NLO corrections reduce the mass scheme uncertainty to approximately half that of the LO [95, 98]. By analogy, we may expect that the mass scheme uncertainty, which we do not assess, is similar in size to our NLO scale uncertainties (see below).

We employ the PDF4LHC15_nlo_30_pdfas PDF set [99] throughout and all of our predictions are at a center of mass energy of $\sqrt{S} = 13$ TeV. Renormalisation and factorisation scales are chosen as

$$\mu_{\text{R,F}} = \xi_{\text{R,F}} \cdot H_T/2, \quad \text{with} \quad H_T = \sqrt{m_H^2 + p_{\text{T,H}}^2} + \sum_j |p_{\text{T,j}}|, \quad (3.1)$$

where the sum includes all final state partons. Our central scale corresponds to $\xi_{\text{R,F}} = (1, 1)$ and we determine scale uncertainties via the standard 7-point factor-2 variations $\xi_{\text{R,F}} = (2, 2), (2, 1), (1, 2), (1, 1), (1, \frac{1}{2}), (\frac{1}{2}, 1), (\frac{1}{2}, \frac{1}{2})$. Any reconstructed jets are clustered via the anti- k_t [100] algorithm with $R = 0.4$. We apply the following cuts:

$$H + \text{jet} : \quad p_{\text{T,j}} > 30 \text{ GeV}, \quad (3.2)$$

$$H + 2\text{jets} : \quad p_{\text{T,j}_1} > 40 \text{ GeV} \text{ and } p_{\text{T,j}_2} > 30 \text{ GeV}. \quad (3.3)$$

The latter asymmetric jet cuts avoid a perturbative instability in the limit $p_{\text{T,H}} \rightarrow 0$ GeV.

3.2 Fiducial total cross sections

Applying the computational setup in Section 3.1, we document the fiducial total cross section for H+jet and H + 2jets production in Tab. 2. For reference we present results for the HTL, FT_{approx} and SM predictions. We also include the fiducial total cross section for boosted Higgs with $p_{T,H} > 300$ GeV. Further fiducial cross sections with varying $p_{T,H}$ cuts are listed in Appendix A. The numbers for H+jet reported here agree, within the statistical uncertainty, with the updated version of Ref. [25].

Together with predictions obtained with the central scale defined in Eq. (3.1) we show the upper and lower values obtained by the envelope of 7-point scale variations. For H+jet production without the fiducial constraint of $p_{T,H}$, the top-quark mass effects lead to an increase of 4.3% (4.6%) at LO (NLO) comparing to HTL. There is an increase of about 1% in the total NLO cross section when comparing the FT_{approx} result with the full top-quark mass dependence. The NLO/LO K-factor is consistent among HTL, FT_{approx} and SM at about 1.65.

With the fiducial constraint of $p_{T,H}$ larger than 300 GeV, we observe a similar amount (2.3%) of relative increase from the FT_{approx} prediction to the result with full top-quark mass effects at NLO.

$\sigma[\text{pb}]$		Inclusive $p_{T,H}$			$p_{T,H} > 300 \text{ GeV}$		
		LO	NLO	K	LO	NLO	K
H+jet	HTL	$8.22^{+3.17}_{-2.15}$	$13.57^{+2.11}_{-2.09}$	1.65	$0.086^{+0.038}_{-0.024}$	$0.160^{+0.033}_{-0.030}$	1.86
	FT _{approx}	$8.56^{+3.30}_{-2.24}$	$14.06(1)^{+2.17}_{-2.16}$	1.64	$0.046^{+0.020}_{-0.013}$	$0.088^{+0.019}_{-0.017}$	1.91
	SM	$8.56^{+3.30}_{-2.24}$	$14.15(7)^{+2.29}_{-2.21}$	1.65	$0.046^{+0.020}_{-0.013}$	$0.089(3)^{+0.020}_{-0.017}$	1.93
H + 2 jets	HTL	$2.87^{+1.67}_{-0.99}$	$4.33^{+0.59}_{-0.80}$	1.51	$0.120^{+0.071}_{-0.042}$	$0.160^{+0.012}_{-0.025}$	1.33
	FT _{approx}	$2.92^{+1.70}_{-1.01}$	$4.45(1)^{+0.63}_{-0.83}$	1.52	$0.068^{+0.040}_{-0.024}$	$0.092^{+0.008}_{-0.015}$	1.35
	SM	$2.92^{+1.70}_{-1.01}$	–	–	$0.068^{+0.040}_{-0.024}$	–	–

Table 2: Integrated cross sections at LO and NLO in the HTL and FT_{approx} approximations and with full top-quark mass dependence (SM) for H+jet and H + 2 jets production together with corresponding K-factors. Uncertainties correspond to the envelope of 7-point scale variations. For H+jet production we require $p_{T,j} > 30 \text{ GeV}$, while for H + 2 jets production we require $p_{T,j_1} > 40 \text{ GeV}$, $p_{T,j_2} > 30 \text{ GeV}$. On the left no further phase-space restrictions are considered, while on the right we additionally require $p_{T,H} > 300 \text{ GeV}$. Numerical integration errors larger than permil level are indicated in brackets.

In contrast, the HTL prediction is 78% (81.8%) larger than the full theory (FT_{approx}) result due to large logarithmic corrections from the disparity in scales between m_t^2 and $p_{T,H}^2$. The NLO/LO K-factor for $p_{T,H} > 300 \text{ GeV}$ is however again almost universal among HTL, FT_{approx} and SM at about 1.9. To be precise, the K-factor in the full SM is 5.3% resp. 2.6% larger compared to the HTL and FT_{approx} predictions.

For H+2 jets production without the fiducial constraint on $p_{T,H}$, the FT_{approx} prediction induces a 1.7% (2.8%) increase compared the HTL approximation at LO (NLO). Considering the fiducial constraint of $p_{T,H}$ larger than 300 GeV, the HTL fiducial total cross section is about 1.76 (1.74) times the FT_{approx} predictions at LO (NLO). However, again in both selections NLO K-factors are universal with mass corrections in the FT_{approx} below the 2% level.

For the absolute cross sections the extra jet emission in H + 2 jets production decreases the total H+jet cross section by more than a factor of 3 from 14.06 pb (H+jet) to 4.45 pb considering the FT_{approx} predictions at NLO in both cases. In contrast, in the boosted Higgs boson regime, the total NLO cross sections are comparable, while the NLO K-factor is about 46% larger in the H+jet computation compared to the H + 2 jets one. This can be understood from the restriction to the back-to-back configuration in the H+jet computation at LO. Multi-jet configurations recoiling against the hard Higgs only open up at NLO, where they are effectively described at LO. In contrast in the H + 2 jets computation such configurations already contribute at LO.

In order to quantify top-quark mass effects in various fiducial regions and to explore the possibility to extrapolate the mass effect to higher order corrections, in the following sections we present in-depth comparisons of differential cross sections for H+jet and H + 2 jets production.

3.3 Fiducial differential cross sections for H+jet production

In Figs. 2-3 we present numerical results for H+jet production at the LHC with $\sqrt{S} = 13 \text{ TeV}$. We compare NLO corrections in the HTL with the FT_{approx} approximation, and with the full SM.

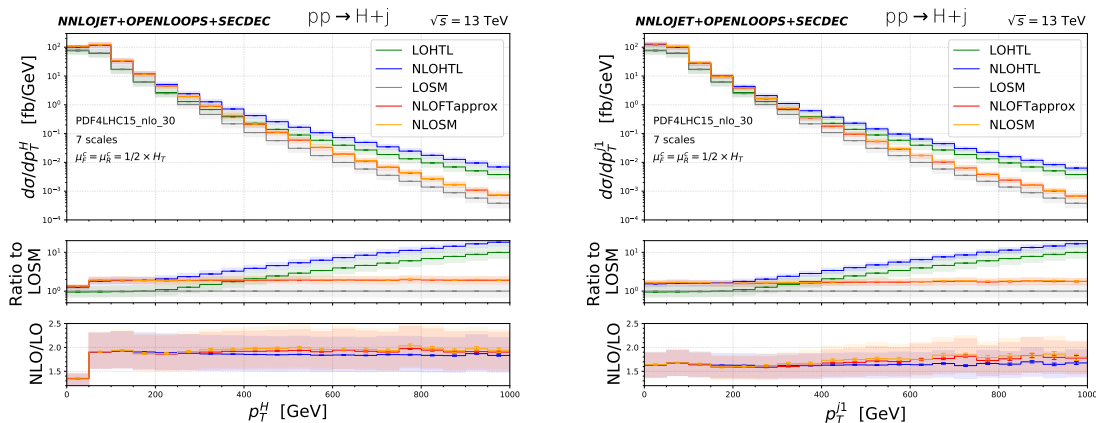


Figure 2: Transverse momentum distribution of the Higgs (left) and the hardest jet (right) in H+jet production. We show LO predictions in the full SM (LOSM, magenta) and the HTL (LOHTL, green) as well as NLO predictions in the HTL (NLOHTL, blue), the FT_{approx} (NLOFTapprox, red) and the full SM (NLOSM, orange). The upper panel shows absolute predictions. The first ratio plot shows corrections with respect to LOSM, while the second ratio plot shows NLO corrections normalised to the respective LO prediction, i.e. $NLOHTL/LOHTL$, $NLOSM/LOSM$, and $NLOFTapprox/LOSM$. Shaded bands correspond to scale variations. Error bars indicate integration uncertainties.

In Fig. 2 we consider the transverse momentum distribution of the Higgs on the left and of the jet on the right. These distributions are identical at LO, and are also highly correlated at NLO. As is well known, for $p_{T,X} > m_t$ ($X = H, j$) the HTL approximation breaks down and predicts a very different high-energy scaling compared to the SM. However, for NLO/LO ratios in the bottom panels of Fig. 2, at least at the $O(10\%)$ level, higher-order QCD corrections in the HTL agree well with the FT_{approx} and the full SM. Further improvement of agreement is observed between the FT_{approx} and the full SM at the $O(5\%)$ level within numerical uncertainties. The scale variation bands in the ratio plots are obtained by fixing the observable at the central scale choice in the denominator while taking the envelope of scale choices in the numerator by the 7-point factor-2 variations. We observe consistent agreement for the size of scale variations also for the ratio plots. In $p_{T,H}$ the corrections are at the level of 90 – 110%, while in $p_{T,j}$ they are at the level of 60 – 80%, for the entire considered range, i.e. shape corrections are mild. Examining the corrections in more detail an overall increase of the corrections of $\approx 5-10\%$ can be appreciated for the full SM compared to the HTL, with a mild relative increase at large transverse momenta slightly larger for $p_{T,j}$ than for $p_{T,H}$. Corrections in the FT_{approx} and the HTL agree exactly up to $p_{T,H}/p_{T,j} \sim m_t$. Beyond that, corrections in the FT_{approx} are a few percent larger compared to the HTL, with again a very slight increase at large transverse momenta. The remaining scale uncertainties at NLO are at the 20 – 25% level throughout.

In Fig. 3 we turn to a different kinematic regime in H+jet production by considering invariant mass distributions in the Higgs-jet system on the left for inclusive H+jet production and on the right considering $p_{T,H} > 300$ GeV. For the inclusive m_{Hj} distribution the HTL NLO result increases mildly by 10 – 20% in the tail of the distribution compared to the FT_{approx} and the full SM. However, the NLO K-factor is universal in all three predictions decreasing from about 1.7 at small m_{Hj} to about 1.5 at large m_{Hj} with similar relative size of scale variation. Finally, in the exclusive $p_{T,H} > 300$ GeV phase-space absolute predictions in the HTL and FT_{approx} diverge for increasing m_{Hj} . However, also here the relative NLO corrections are found to be largely identical for the HTL,

$\text{FT}_{\text{approx}}$ and full top-quark mass results. This holds at large m_{Hj} as well as at small m_{Hj} , which for $m_{Hj} < 600$ GeV is kinematically inaccessible at LO due to the $p_{T,H} > 300$ GeV requirement.

From the detailed comparison of $p_{T,H}$, $p_{T,j}$ and m_{Hj} distributions of H+jet production, we observe excellent agreement of differential NLO/LO K-factors (for the central scale and scale variations) among theory predictions using HTL, $\text{FT}_{\text{approx}}$ and the exact top-quark mass dependence. This observation validates the multiplicative reweighting procedure introduced in [47] at histogram level and further strengthens the reweighted predictions for H+jet production at NNLO accuracy [15].

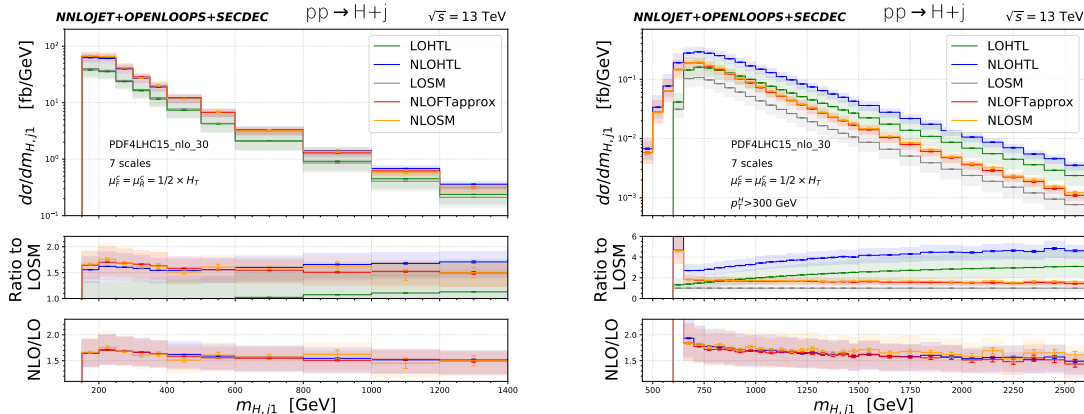


Figure 3: Invariant mass distribution of the Higgs and the jet for inclusive H+jet production (left) and with $p_{T,H} > 300$ GeV (right). Colour coding and labelling as in Fig. 2.

3.4 Fiducial differential cross sections for H + 2jets production

In Figs. 4-7 we turn to the numerical results for H+2jets production. We compare NLO corrections in the HTL with the $\text{FT}_{\text{approx}}$ approximation, focussing on multi-jet observables and jet correlations with and without boosted Higgs kinematics (i.e. inclusive and with an additional $p_{T,H} > 300$ GeV requirement). As discussed in the introduction these are phenomenologically highly relevant for the modelling of H + 2jets backgrounds in analyses for VBF Higgs production.

In Fig. 4 we consider the transverse momentum of the Higgs (left) and of the hardest jet (right). These plots can directly be compared with the corresponding ones for H+jet production in Fig. 2. Again we observe very large deviations of the nominal predictions at large transverse momenta. At the same time also the QCD corrections are sizeable: around 60–70% at small p_T and around 30% for $p_{T,H}/p_{T,j} = 1$ TeV. However the relative NLO corrections normalised to the respective LO show a universal behaviour, i.e. they are identical in the HTL and the $\text{FT}_{\text{approx}}$.

A similar picture as for the transverse momentum distributions emerges when looking at the distribution in the invariant mass of the Higgs and the hardest jet, as depicted in Fig. 5. Both, for the inclusive selection (as shown on the left), and for the boosted Higgs selection with an additional $p_{T,H} > 300$ GeV requirement, the QCD corrections in the $\text{FT}_{\text{approx}}$ identically track the corresponding corrections in the HTL, while the nominal predictions substantially diverge.

Next, in Fig. 6 we turn to the phenomenologically important dijet invariant mass distribution. Again we consider an inclusive selection (left) and a boosted selection requiring $p_{T,H} > 300$ GeV. In the inclusive phase-space the NLO corrections are about 50% in the $\text{FT}_{\text{approx}}$ with hardly any variations over the considered $m_{j_1 j_2}$ range. Corrections in the HTL are identical to the $\text{FT}_{\text{approx}}$ at small $m_{j_1 j_2}$ and slightly reduce to about 40% in the multi TeV range, i.e. up to 10% smaller than

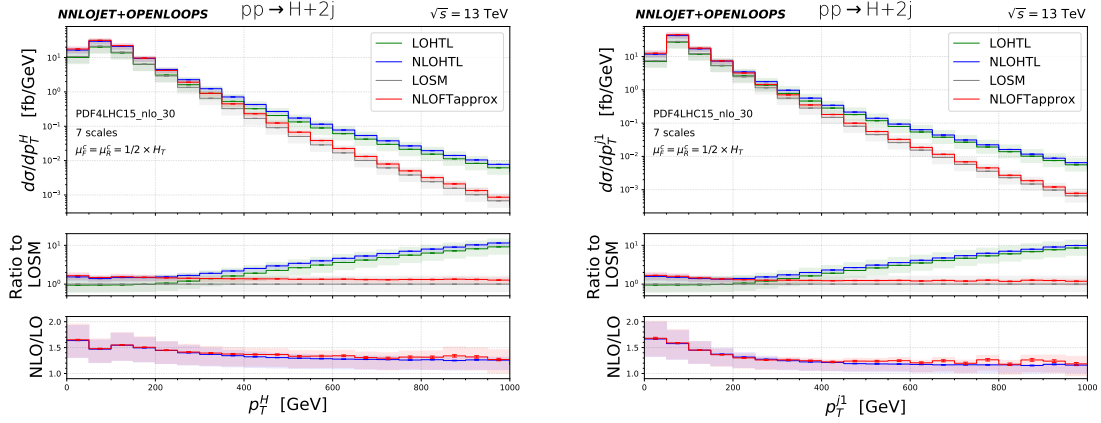


Figure 4: Transverse momentum distribution of the Higgs (left) and the hardest jet (right) in $H + 2$ jets production. Colour coding and labelling as in Fig. 2.

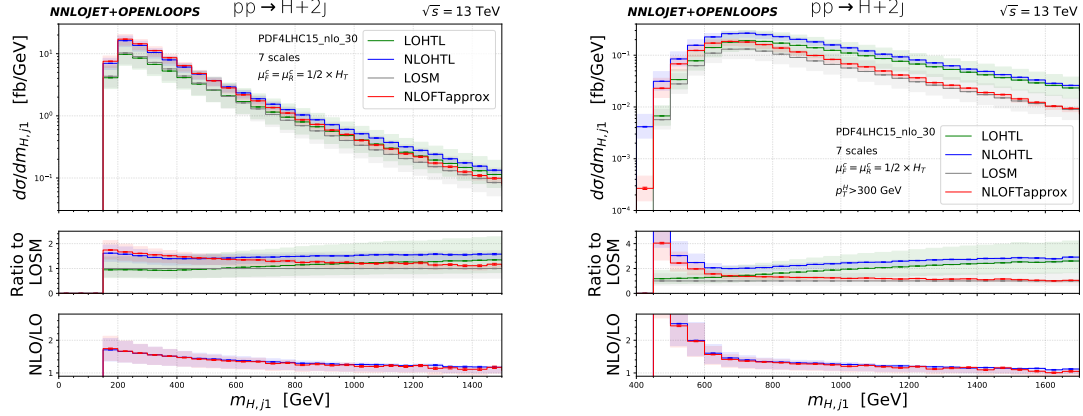


Figure 5: Invariant mass distribution of the Higgs and the hardest jet system in $H + 2$ jets production. Colour coding and labelling as in Fig. 2.

in the FT_{approx} . With the boosted selection, corrections in both the FT_{approx} and the HTL are at the level of 30 – 40% and marginally reduce in the tail of the $m_{j_1 j_2}$ distribution.

Finally in Fig. 7 we plot the rapidity difference between the two jets in $H + 2$ jets production, again with an inclusive selection on the left and a boosted selection on the right. In the inclusive case there is hardly any variation in the NLO corrections over the considered rapidity range with a K-factor at the 1.5 level. For the boosted selection, the K-factor decreases slightly from about 1.35 to 1.25 from small to high rapidity differences. For both selections and over the entire rapidity range corrections in the FT_{approx} and the HTL agree at the percent level. We observed very similar findings also in other angular correlation observables including e.g. the rapidity difference between the Higgs and the hardest jet.

Overall in all considered observables we find a remarkable agreement of the relative corrections computed in the HTL and the FT_{approx} — despite up to several order of magnitude variations in nominal predictions. This clearly points towards a factorisation of QCD higher-order corrections from the heavy fermion loop mediating the coupling of the Higgs boson.

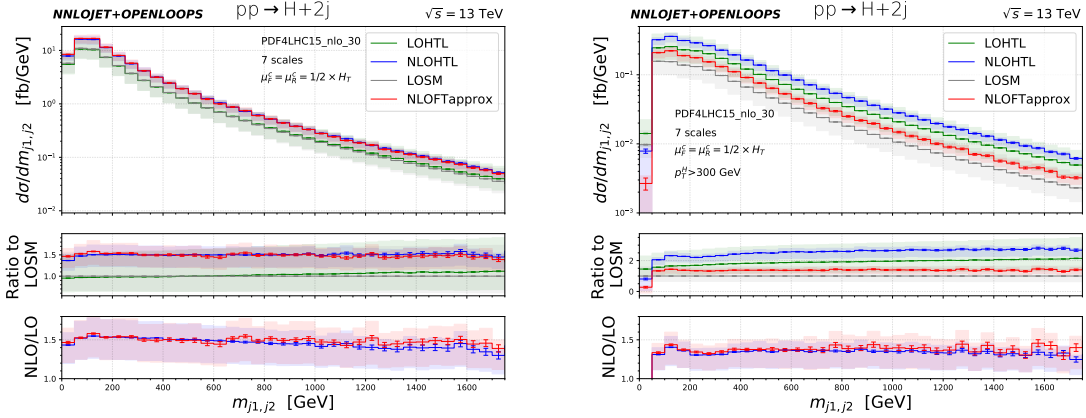


Figure 6: Invariant mass distribution of the di-jet system in $H + 2$ jets production. Colour coding and labelling as in Fig. 2.

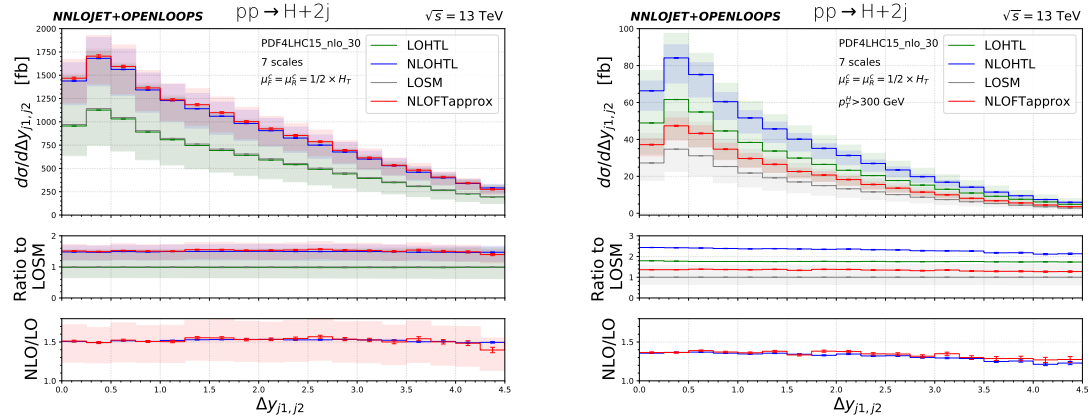


Figure 7: Rapidity difference between the two hardest jets in $H + 2$ jets production. Colour coding and labelling as in Fig. 2.

4 Conclusions

In this paper we have presented precise differential predictions for $H + \text{jet}$ and $H + 2$ jets production at the LHC at NLO including top-quark mass effects. For the former process our prediction incorporates the exact top-quark mass dependence. Instead, in our study of $H + 2$ jets production, the two-loop virtual matrix elements are computed in the HTL approximation (infinite top-quark mass) and reweighed by the full LO result, while the exact top-quark mass dependence is retained in the Born and real radiation contributions. Our results are produced using the NNLOJET event generator with one-loop amplitudes provided by OPENLOOPS2.2 (to be released soon) which implements a novel tensor reduction method based on the on-the-fly reduction algorithm of OpenLoops. The two-loop virtual matrix elements including top-quark mass effects contributing to $H + \text{jet}$ production are evaluated using SECDEC-3.

We find that the inclusion of the exact top-quark mass dependence in the two-loop virtual matrix elements enhances the cross section for $H + \text{jet}$ production at NLO by about 0.6% with respect to the $\text{FT}_{\text{approx}}$ prediction, and by about 4.3% with respect to the HTL prediction. However, the

NLO/LO K-factor is found to be universal amongst the three predictions at about 1.7. Noteworthy, this universality is broadly also found examining the corrections to the $p_{T,H}$ and $p_{T,j}$ distributions. Although above the top-quark threshold the HTL approximation becomes formally invalid, relative NLO corrections agree at the 10% (5%) level between HTL ($\text{FT}_{\text{approx}}$) respectively and the full theory.

Regarding the $H + 2\text{jets}$ production process we have produced distributions for the p_T of the Higgs boson and leading jet as well as invariant mass distributions for the Higgs + leading jet system and the leading dijet system. In particular the latter is crucial for gluon-fusion Higgs production backgrounds in VBF Higgs production analyses. At the inclusive level the $\text{FT}_{\text{approx}}$ cross section is 2.8% larger than the HTL prediction. Differentially, we observe that the approximate inclusion of the top-quark mass has the largest, though still rather mild, impact on the p_T distributions above the top-quark threshold. Relative higher-order corrections in the HTL and the $\text{FT}_{\text{approx}}$ always agree at below the 10% level.

Overall, the top-quark mass effects at NLO are observed to be rather mild. In particular they are expected to be at the same level or even smaller than the current uncertainties due to the scheme dependence of the top-quark mass.

The computations presented are relevant for analyses of Higgs production at large transverse momentum and also for Higgs plus multi-jet backgrounds in Higgs production via vector boson fusion. Through detailed comparisons, this study proves the reliability of higher-order corrections computed in the HTL rescaled with lower-order predictions with explicit mass dependence. The multiplicative reweighting procedures are of similar theoretical uncertainties, within 10%, for both event-by-event and bin-by-bin rescaling. This paves the way towards computations of $pp \rightarrow H + j$ including approximate mass effects at NNLO and higher QCD accuracy.

Acknowledgments

We are grateful to Alexander Karlberg for contributions at the early stage of this work. We thank Thomas Gehrmann, Gudrun Heinrich, Joey Huston and Stefano Pozzorini for useful discussions and comments on the manuscript. We thank the University of Zurich S3IT (<http://www.s3it.uzh.ch>) and Swiss National Supercomputing Centre (CSCS) for providing support and computational resources. This research is supported in part by the Swiss National Science Foundation (SNF) under contract 200020-175595 and by CSCS under project ID UZH10. This research was supported in parts by the Deutsche Forschungsgemeinschaft (DFG, German Research Foundation) under grant 396021762 - TRR 257. J.L. is supported by the Science and Technology Research Council (STFC) under the Consolidated Grant ST/T00102X/1 and the STFC Ernest Rutherford Fellowship ST/S005048/1. S.P.J. is supported by a Royal Society University Research Fellowship (Grant URF/R1/201268). J.-N.L. and H.Z. are supported by the Swiss National Science Foundation (SNF) under contract BSCGI0-157722.

A Inclusive cross sections

In Tab. 3 and Tab. 4 we list as reference integrated cross sections $\sigma(p_{T,H} > p_{T,H}^{\text{cut}})$ in function of $p_{T,H}^{\text{cut}}$ for $pp \rightarrow H + j$ and $pp \rightarrow H + jj$ respectively. Shown are cross sections at LO and NLO and related K-factors considering the HTL and $\text{FT}_{\text{approx}}$ approximations, and for $pp \rightarrow H + j$ also the results with exact top-mass dependence. The setup is given in Section 3.1.

$p_{T,H}^{\text{cut}}$	LO _{HTL}	NLO _{HTL}	K _{HTL} ^{NLO}	LO _{SM}	NLO _{FT_{approx}}	K _{FT_{approx}} ^{NLO}	NLO _{SM}	K _{SM} ^{NLO}
50	4453 ⁺¹⁷⁵⁵ ₋₁₁₈₁	8482 ⁺¹⁷⁵⁵ ₋₁₅₂₂	1.90	4566 ⁺¹⁸⁰⁰ ₋₁₂₁₂	8682 ⁺¹⁷⁹³ ₋₁₅₅₇	1.90	8732 ⁺¹⁸⁵⁸ ₋₁₅₈₅	1.91
100	1430 ⁺⁵⁸⁵ ₋₃₈₉	2732 ⁺⁵⁷⁸ ₋₅₀₂	1.91	1391 ⁺⁵⁷⁰ ₋₃₇₉	2645 ⁺⁵⁵⁷ ₋₄₈₅	1.90	2669 ⁺⁵⁷⁵ ₋₄₉₄	1.92
150	593 ⁺²⁴⁹ ₋₁₆₄	1121 ⁺²³⁵ ₋₂₀₇	1.89	528 ⁺²²² ₋₁₄₆	989 ⁺²⁰⁵ ₋₁₈₂	1.87	996 ⁺²¹⁶ ₋₁₈₆	1.89
200	284 ⁺¹²¹ _{-79.6}	533 ⁺¹¹¹ _{-98.9}	1.88	219 ^{+94.2} _{-61.7}	411 ^{+85.9} _{-76.5}	1.88	417 ^{+90.0} _{-78.4}	1.90
250	151 ^{+65.2} _{-42.6}	281 ^{+58.2} _{-52.2}	1.87	97.4 ^{+42.5} _{-27.7}	184 ^{+39.3} _{-34.8}	1.89	189 ^{+41.2} _{-36.1}	1.94
300	85.9 ^{+37.6} _{-24.5}	160 ^{+32.9} _{-29.7}	1.86	45.9 ^{+20.3} _{-13.2}	87.8 ^{+19.2} _{-16.9}	1.91	90.1 ^{+19.7} _{-17.4}	1.96
350	51.8 ^{+22.9} _{-14.8}	95.9 ^{+19.7} _{-17.9}	1.85	22.9 ^{+10.2} _{-6.62}	44.0 ^{+9.71} _{-8.53}	1.92	45.1 ^{+10.2} _{-8.85}	1.97
400	32.5 ^{+14.5} _{-9.38}	60.1 ^{+12.3} _{-11.2}	1.85	12.0 ^{+5.39} _{-3.48}	23.0 ^{+5.10} _{-4.49}	1.92	23.6 ^{+5.38} _{-4.66}	1.98
450	21.2 ^{+9.49} _{-6.14}	39.1 ^{+8.00} _{-7.33}	1.84	6.52 ^{+2.96} _{-1.91}	12.6 ^{+2.80} _{-2.46}	1.93	12.9 ^{+2.97} _{-2.56}	1.98
500	14.2 ^{+6.39} _{-4.13}	26.2 ^{+5.36} _{-4.92}	1.84	3.67 ^{+1.68} _{-1.08}	7.09 ^{+1.59} _{-1.40}	1.93	7.25 ^{+1.69} _{-1.45}	1.97
550	9.71 ^{+4.40} _{-2.84}	17.9 ^{+3.66} _{-3.37}	1.84	2.14 ^{+0.98} _{-0.63}	4.11 ^{+0.92} _{-0.81}	1.92	4.18 ^{+0.96} _{-0.83}	1.96
600	6.79 ^{+3.09} _{-1.99}	12.5 ^{+2.56} _{-2.36}	1.84	1.28 ^{+0.59} _{-0.38}	2.47 ^{+0.56} _{-0.49}	1.93	2.50 ^{+0.59} _{-0.51}	1.96
650	4.82 ^{+2.21} _{-1.42}	8.88 ^{+1.83} _{-1.69}	1.84	0.78 ^{+0.36} _{-0.23}	1.50 ^{+0.34} _{-0.30}	1.92	1.53 ^{+0.36} _{-0.31}	1.96
700	3.48 ^{+1.60} _{-1.03}	6.42 ^{+1.33} _{-1.22}	1.85	0.49 ^{+0.23} _{-0.15}	0.94 ^{+0.21} _{-0.19}	1.92	0.96 ^{+0.23} _{-0.19}	1.96
750	2.54 ^{+1.17} _{-0.75}	4.68 ^{+0.97} _{-0.89}	1.84	0.31 ^{+0.15} _{-0.09}	0.60 ^{+0.14} _{-0.12}	1.94	0.62 ^{+0.14} _{-0.13}	1.97
800	1.87 ^{+0.87} _{-0.56}	3.45 ^{+0.71} _{-0.66}	1.84	0.20 ^{+0.1} _{-0.06}	0.39 ^{+0.09} _{-0.08}	1.92	0.39 ^{+0.09} _{-0.08}	1.94

Table 3: Integrated cross sections in fb depending on $p_{T,H}^{\text{cut}}$ at LO and NLO in the HTL, FT_{approx}, and with full top-quark mass dependence (SM) for H+jet production at the LHC with $\sqrt{S} = 13$ TeV together with corresponding K-factors. Uncertainties correspond to the envelope of 7-point scale variations. We require $p_{T,j} > 30$ GeV.

$p_{T,H}^{\text{cut}}$	LO _{HTL}	NLO _{HTL}	K _{HTL} ^{NLO}	LO _{SM}	NLO _{FT_{approx}}	K _{FT_{approx}} ^{NLO}
50	2365 ⁺¹³⁷⁷ ₋₈₁₃	3511 ⁺⁴⁴⁶ ₋₆₃₁	1.48	2387 ⁺¹³⁹¹ ₋₈₂₁	3574 ⁺⁴⁷⁷ ₋₆₅₁	1.50
100	1355 ⁺⁷⁹⁰ ₋₄₆₆	2025 ⁺²⁶⁷ ₋₃₆₈	1.50	1317 ⁺⁷⁶⁹ ₋₄₅₄	1991 ⁺²⁷⁶ ₋₃₆₈	1.51
150	671 ⁺³⁹² ₋₂₃₂	969 ⁺¹¹⁰ ₋₁₆₉	1.44	601 ⁺³⁵³ ₋₂₀₈	881 ⁺¹⁰⁷ ₋₁₅₇	1.47
200	355 ⁺²⁰⁸ ₋₁₂₃	497 ^{+47.9} _{-83.4}	1.40	281 ⁺¹⁶⁶ _{-97.5}	399 ^{+42.1} _{-68.7}	1.42
250	201 ⁺¹¹⁸ _{-69.6}	274 ^{+22.7} _{-44.4}	1.36	136 ^{+80.2} _{-47.2}	188 ^{+17.8} _{-31.6}	1.39
300	120 ^{+70.5} _{-41.6}	160 ^{+11.8} _{-25.3}	1.34	68.1 ^{+40.3} _{-23.7}	92.4 ^{+7.73} _{-15.2}	1.36
350	74.8 ^{+44.0} _{-26.0}	98.5 ^{+6.53} _{-15.2}	1.32	35.5 ^{+21.1} _{-12.4}	47.7 ^{+3.70} _{-7.73}	1.34
400	48.4 ^{+28.5} _{-16.8}	62.9 ^{+3.82} _{-9.56}	1.30	19.2 ^{+11.4} _{-6.71}	25.4 ^{+1.82} _{-4.05}	1.33
450	32.2 ^{+19.0} _{-11.2}	41.5 ^{+2.36} _{-6.23}	1.29	10.7 ^{+6.38} _{-3.75}	14.1 ^{+0.96} _{-2.23}	1.32
500	21.9 ^{+12.9} _{-7.62}	28.0 ^{+1.51} _{-4.18}	1.28	6.16 ^{+3.68} _{-2.16}	8.06 ^{+0.52} _{-1.27}	1.31
550	15.2 ^{+8.99} _{-5.30}	19.4 ^{+1.01} _{-2.87}	1.27	3.64 ^{+2.18} _{-1.28}	4.74 ^{+0.30} _{-0.74}	1.30
600	10.8 ^{+6.37} _{-3.75}	13.7 ^{+0.69} _{-2.02}	1.27	2.20 ^{+1.32} _{-0.77}	2.85 ^{+0.18} _{-0.44}	1.29
650	7.72 ^{+4.57} _{-2.70}	9.79 ^{+0.49} _{-1.44}	1.27	1.36 ^{+0.82} _{-0.48}	1.76 ^{+0.11} _{-0.27}	1.29
700	5.61 ^{+3.33} _{-1.96}	7.10 ^{+0.35} _{-1.05}	1.27	0.85 ^{+0.51} _{-0.30}	1.10 ^{+0.07} _{-0.17}	1.29
750	4.12 ^{+2.45} _{-1.44}	5.22 ^{+0.25} _{-0.77}	1.26	0.55 ^{+0.33} _{-0.19}	0.70 ^{+0.04} _{-0.11}	1.29
800	3.06 ^{+1.82} _{-1.07}	3.88 ^{+0.19} _{-0.57}	1.27	0.36 ^{+0.22} _{-0.13}	0.46 ^{+0.03} _{-0.07}	1.28

Table 4: Integrated cross sections in fb depending on $p_{T,H}^{\text{cut}}$ at LO and NLO in the HTL and FT_{approx} for H + 2jets production at the LHC with $\sqrt{S} = 13$ TeV together with corresponding K-factors. Uncertainties correspond to the envelope of 7-point scale variations. We require $p_{T,j_1} > 40$ GeV, $p_{T,j_2} > 30$ GeV.

References

- [1] C. Arnesen, I. Z. Rothstein, and J. Zupan, *Smoking Guns for On-Shell New Physics at the LHC*, *Phys. Rev. Lett.* **103** (2009) 151801, [[arXiv:0809.1429](#)].
- [2] A. Banfi, A. Martin, and V. Sanz, *Probing top-partners in Higgs+jets*, *JHEP* **08** (2014) 053, [[arXiv:1308.4771](#)].
- [3] A. Azatov and A. Paul, *Probing Higgs couplings with high p_T Higgs production*, *JHEP* **01** (2014) 014, [[arXiv:1309.5273](#)].
- [4] C. Grojean, E. Salvioni, M. Schlaffer, and A. Weiler, *Very boosted Higgs in gluon fusion*, *JHEP* **05** (2014) 022, [[arXiv:1312.3317](#)].
- [5] R. V. Harlander and T. Neumann, *Probing the nature of the Higgs-gluon coupling*, *Phys. Rev. D* **88** (2013) 074015, [[arXiv:1308.2225](#)].
- [6] S. Dawson, I. M. Lewis, and M. Zeng, *Effective field theory for Higgs boson plus jet production*, *Phys. Rev. D* **90** (2014), no. 9 093007, [[arXiv:1409.6299](#)].
- [7] U. Langenegger, M. Spira, and I. Strebel, *Testing the Higgs Boson Coupling to Gluons*, [arXiv:1507.01373](#).
- [8] M. Grazzini, A. Ilnicka, M. Spira, and M. Wiesemann, *Modeling BSM effects on the Higgs transverse-momentum spectrum in an EFT approach*, *JHEP* **03** (2017) 115, [[arXiv:1612.00283](#)].
- [9] N. Deutschmann, C. Duhr, F. Maltoni, and E. Vryonidou, *Gluon-fusion Higgs production in the Standard Model Effective Field Theory*, *JHEP* **12** (2017) 063, [[arXiv:1708.00460](#)]. [Erratum: *JHEP* **02**, 159 (2018)].
- [10] M. Battaglia, M. Grazzini, M. Spira, and M. Wiesemann, *Sensitivity to BSM effects in the Higgs p_T spectrum within SMEFT*, [arXiv:2109.02987](#).
- [11] ATLAS Collaboration, *Prospects for differential cross-section measurements of Higgs boson production measured in decays to ZZ and $\gamma\gamma$ with the ATLAS experiment at the High-Luminosity LHC*, *ATL-PHYS-PUB-2018-040* (2018).
- [12] CMS Collaboration, *Sensitivity projections for Higgs boson properties measurements at the HL-LHC*, *CMS-PAS-FTR-18-011* (2018).
- [13] ATLAS Collaboration, *Study of Higgs-boson production with large transverse momentum using the $H \rightarrow b\bar{b}$ decay with the ATLAS detector*, *ATLAS-CONF-2021-010* (3, 2021).
- [14] CMS Collaboration, A. M. Sirunyan et al., *Inclusive search for highly boosted Higgs bosons decaying to bottom quark-antiquark pairs in proton-proton collisions at $\sqrt{s} = 13$ TeV*, *JHEP* **12** (2020) 085, [[arXiv:2006.13251](#)].
- [15] K. Becker et al., *Precise predictions for boosted Higgs production*, [arXiv:2005.07762](#).
- [16] F. Campanario, T. M. Figy, S. Plätzer, M. Rauch, P. Schichtel, and M. Sjö Dahl, *Stress testing the vector-boson-fusion approximation in multijet final states*, *Phys. Rev. D* **98** (2018), no. 3 033003, [[arXiv:1802.09955](#)].
- [17] A. Buckley et al., *A comparative study of Higgs boson production from vector-boson fusion*, [arXiv:2105.11399](#).
- [18] P. Artoisenet et al., *A framework for Higgs characterisation*, *JHEP* **11** (2013) 043, [[arXiv:1306.6464](#)].
- [19] F. Maltoni, K. Mawatari, and M. Zaro, *Higgs characterisation via vector-boson fusion and associated production: NLO and parton-shower effects*, *Eur. Phys. J. C* **74** (2014), no. 1 2710, [[arXiv:1311.1829](#)].
- [20] A. Greljo, G. Isidori, J. M. Lindert, and D. Marzocca, *Pseudo-observables in electroweak Higgs production*, *Eur. Phys. J. C* **76** (2016), no. 3 158, [[arXiv:1512.06135](#)].

- [21] C. Degrande, B. Fuks, K. Mawatari, K. Mimasu, and V. Sanz, *Electroweak Higgs boson production in the standard model effective field theory beyond leading order in QCD*, *Eur. Phys. J. C* **77** (2017), no. 4 262, [[arXiv:1609.04833](#)].
- [22] A. Greljo, G. Isidori, J. M. Lindert, D. Marzocca, and H. Zhang, *Electroweak Higgs production with HiggsPO at NLO QCD*, *Eur. Phys. J. C* **77** (2017), no. 12 838, [[arXiv:1710.04143](#)].
- [23] J. Y. Araz, S. Banerjee, R. S. Gupta, and M. Spannowsky, *Precision SMEFT bounds from the VBF Higgs at high transverse momentum*, *JHEP* **04** (2021) 125, [[arXiv:2011.03555](#)].
- [24] M. Czakon, R. V. Harlander, J. Klappert, and M. Niggetiedt, *Exact top-quark mass dependence in hadronic Higgs production*, [arXiv:2105.04436](#).
- [25] S. P. Jones, M. Kerner, and G. Luisoni, *Next-to-Leading-Order QCD Corrections to Higgs Boson Plus Jet Production with Full Top-Quark Mass Dependence*, *Phys. Rev. Lett.* **120** (2018), no. 16 162001, [[arXiv:1802.00349](#)].
- [26] J. M. Lindert, K. Kudashkin, K. Melnikov, and C. Wever, *Higgs bosons with large transverse momentum at the LHC*, *Phys. Lett. B* **782** (2018) 210–214, [[arXiv:1801.08226](#)].
- [27] T. Neumann, *NLO Higgs+jet production at large transverse momenta including top quark mass effects*, *J. Phys. Comm.* **2** (2018), no. 9 095017, [[arXiv:1802.02981](#)].
- [28] M. Kerner, *Top mass effects in HJ and HH production*, *PoS RADCOR2019* (2019) 020.
- [29] V. Del Duca, W. Kilgore, C. Oleari, C. Schmidt, and D. Zeppenfeld, *Higgs + 2 jets via gluon fusion*, *Phys. Rev. Lett.* **87** (2001) 122001, [[hep-ph/0105129](#)].
- [30] V. Del Duca, W. Kilgore, C. Oleari, C. Schmidt, and D. Zeppenfeld, *Gluon fusion contributions to H + 2 jet production*, *Nucl. Phys. B* **616** (2001) 367–399, [[hep-ph/0108030](#)].
- [31] T. Neumann and C. Williams, *The Higgs boson at high p_T* , *Phys. Rev. D* **95** (2017), no. 1 014004, [[arXiv:1609.00367](#)].
- [32] J. R. Andersen, J. D. Cockburn, M. Heil, A. Maier, and J. M. Smillie, *Finite Quark-Mass Effects in Higgs Boson Production with Dijets at Large Energies*, *JHEP* **04** (2019) 127, [[arXiv:1812.08072](#)].
- [33] L. Budge, J. M. Campbell, G. De Laurentis, R. K. Ellis, and S. Seth, *The one-loop amplitudes for Higgs + 4 partons with full mass effects*, *JHEP* **05** (2020) 079, [[arXiv:2002.04018](#)].
- [34] S. Borowka, G. Heinrich, S. P. Jones, M. Kerner, J. Schlenk, and T. Zirke, *SecDec-3.0: numerical evaluation of multi-scale integrals beyond one loop*, *Comput. Phys. Commun.* **196** (2015) 470–491, [[arXiv:1502.06595](#)].
- [35] S. Borowka, G. Heinrich, S. Jahn, S. P. Jones, M. Kerner, J. Schlenk, and T. Zirke, *pySecDec: a toolbox for the numerical evaluation of multi-scale integrals*, *Comput. Phys. Commun.* **222** (2018) 313–326, [[arXiv:1703.09692](#)].
- [36] K. Kudashkin, K. Melnikov, and C. Wever, *Two-loop amplitudes for processes $gg \rightarrow Hg, qg \rightarrow Hq$ and $q\bar{q} \rightarrow Hg$ at large Higgs transverse momentum*, *JHEP* **02** (2018) 135, [[arXiv:1712.06549](#)].
- [37] F. Wilczek, *Decays of Heavy Vector Mesons Into Higgs Particles*, *Phys. Rev. Lett.* **39** (1977) 1304.
- [38] C. Anastasiou, C. Duhr, F. Dulat, F. Herzog, and B. Mistlberger, *Higgs Boson Gluon-Fusion Production in QCD at Three Loops*, *Phys. Rev. Lett.* **114** (2015) 212001, [[arXiv:1503.06056](#)].
- [39] F. Dulat, B. Mistlberger, and A. Pelloni, *Differential Higgs production at N^3 LO beyond threshold*, *JHEP* **01** (2018) 145, [[arXiv:1710.03016](#)].
- [40] L. Cieri, X. Chen, T. Gehrmann, E. W. N. Glover, and A. Huss, *Higgs boson production at the LHC using the q_T subtraction formalism at N^3 LO QCD*, *JHEP* **02** (2019) 096, [[arXiv:1807.11501](#)].
- [41] B. Mistlberger, *Higgs boson production at hadron colliders at N^3 LO in QCD*, *JHEP* **05** (2018) 028, [[arXiv:1802.00833](#)].

- [42] X. Chen, T. Gehrmann, E. W. N. Glover, A. Huss, B. Mistlberger, and A. Pelloni, *Fully Differential Higgs Boson Production to Third Order in QCD*, *Phys. Rev. Lett.* **127** (2021), no. 7 072002, [[arXiv:2102.07607](#)].
- [43] R. Boughezal, F. Caola, K. Melnikov, F. Petriello, and M. Schulze, *Higgs boson production in association with a jet at next-to-next-to-leading order in perturbative QCD*, *JHEP* **06** (2013) 072, [[arXiv:1302.6216](#)].
- [44] X. Chen, T. Gehrmann, E. W. N. Glover, and M. Jaquier, *Precise QCD predictions for the production of Higgs + jet final states*, *Phys. Lett. B* **740** (2015) 147–150, [[arXiv:1408.5325](#)].
- [45] R. Boughezal, F. Caola, K. Melnikov, F. Petriello, and M. Schulze, *Higgs boson production in association with a jet at next-to-next-to-leading order*, *Phys. Rev. Lett.* **115** (2015), no. 8 082003, [[arXiv:1504.07922](#)].
- [46] R. Boughezal, C. Focke, W. Giele, X. Liu, and F. Petriello, *Higgs boson production in association with a jet at NNLO using jetiness subtraction*, *Phys. Lett. B* **748** (2015) 5–8, [[arXiv:1505.03893](#)].
- [47] X. Chen, J. Cruz-Martinez, T. Gehrmann, E. W. N. Glover, and M. Jaquier, *NNLO QCD corrections to Higgs boson production at large transverse momentum*, *JHEP* **10** (2016) 066, [[arXiv:1607.08817](#)].
- [48] J. M. Campbell, R. K. Ellis, and G. Zanderighi, *Next-to-Leading order Higgs + 2 jet production via gluon fusion*, *JHEP* **10** (2006) 028, [[hep-ph/0608194](#)].
- [49] H. van Deurzen, N. Greiner, G. Luisoni, P. Mastrolia, E. Mirabella, G. Ossola, T. Peraro, J. F. von Soden-Fraunhofen, and F. Tramontano, *NLO QCD corrections to the production of Higgs plus two jets at the LHC*, *Phys. Lett. B* **721** (2013) 74–81, [[arXiv:1301.0493](#)].
- [50] G. Cullen, H. van Deurzen, N. Greiner, G. Luisoni, P. Mastrolia, E. Mirabella, G. Ossola, T. Peraro, and F. Tramontano, *Next-to-Leading-Order QCD Corrections to Higgs Boson Production Plus Three Jets in Gluon Fusion*, *Phys. Rev. Lett.* **111** (2013), no. 13 131801, [[arXiv:1307.4737](#)].
- [51] G. Bozzi, S. Catani, D. de Florian, and M. Grazzini, *Transverse-momentum resummation and the spectrum of the Higgs boson at the LHC*, *Nucl. Phys. B* **737** (2006) 73–120, [[hep-ph/0508068](#)].
- [52] D. de Florian, G. Ferrera, M. Grazzini, and D. Tommasini, *Transverse-momentum resummation: Higgs boson production at the Tevatron and the LHC*, *JHEP* **11** (2011) 064, [[arXiv:1109.2109](#)].
- [53] T. Becher, M. Neubert, and D. Wilhelm, *Higgs-Boson Production at Small Transverse Momentum*, *JHEP* **05** (2013) 110, [[arXiv:1212.2621](#)].
- [54] W. Bizon, P. F. Monni, E. Re, L. Rottoli, and P. Torrielli, *Momentum-space resummation for transverse observables and the Higgs p_{\perp} at $N^3LL+NNLO$* , *JHEP* **02** (2018) 108, [[arXiv:1705.09127](#)].
- [55] X. Chen, T. Gehrmann, E. W. N. Glover, A. Huss, Y. Li, D. Neill, M. Schulze, I. W. Stewart, and H. X. Zhu, *Precise QCD Description of the Higgs Boson Transverse Momentum Spectrum*, *Phys. Lett. B* **788** (2019) 425–430, [[arXiv:1805.00736](#)].
- [56] W. Bizoń, X. Chen, A. Gehrmann-De Ridder, T. Gehrmann, N. Glover, A. Huss, P. F. Monni, E. Re, L. Rottoli, and P. Torrielli, *Fiducial distributions in Higgs and Drell-Yan production at $N^3LL+NNLO$* , *JHEP* **12** (2018) 132, [[arXiv:1805.05916](#)].
- [57] E. Re, L. Rottoli, and P. Torrielli, *Fiducial Higgs and Drell-Yan distributions at $N^3LL'+NNLO$ with RadISH*, [[arXiv:2104.07509](#)].
- [58] H. Mantler and M. Wiesemann, *Top- and bottom-mass effects in hadronic Higgs production at small transverse momenta through $LO+NLL$* , *Eur. Phys. J. C* **73** (2013), no. 6 2467, [[arXiv:1210.8263](#)].
- [59] M. Grazzini and H. Sargsyan, *Heavy-quark mass effects in Higgs boson production at the LHC*, *JHEP* **09** (2013) 129, [[arXiv:1306.4581](#)].

- [60] A. Banfi, P. F. Monni, and G. Zanderighi, *Quark masses in Higgs production with a jet veto*, *JHEP* **01** (2014) 097, [[arXiv:1308.4634](#)].
- [61] K. Melnikov, L. Tancredi, and C. Wever, *Two-loop $gg \rightarrow Hg$ amplitude mediated by a nearly massless quark*, *JHEP* **11** (2016) 104, [[arXiv:1610.03747](#)].
- [62] J. M. Lindert, K. Melnikov, L. Tancredi, and C. Wever, *Top-bottom interference effects in Higgs plus jet production at the LHC*, *Phys. Rev. Lett.* **118** (2017), no. 25 252002, [[arXiv:1703.03886](#)].
- [63] K. Melnikov, L. Tancredi, and C. Wever, *Two-loop amplitudes for $q\bar{q} \rightarrow Hq$ and $q\bar{q} \rightarrow Hg$ mediated by a nearly massless quark*, *Phys. Rev. D* **95** (2017), no. 5 054012, [[arXiv:1702.00426](#)].
- [64] F. Caola, J. M. Lindert, K. Melnikov, P. F. Monni, L. Tancredi, and C. Wever, *Bottom-quark effects in Higgs production at intermediate transverse momentum*, *JHEP* **09** (2018) 035, [[arXiv:1804.07632](#)].
- [65] F. Caola, S. Forte, S. Marzani, C. Muselli, and G. Vita, *The Higgs transverse momentum spectrum with finite quark masses beyond leading order*, *JHEP* **08** (2016) 150, [[arXiv:1606.04100](#)].
- [66] R. V. Harlander, T. Neumann, K. J. Ozeren, and M. Wiesemann, *Top-mass effects in differential Higgs production through gluon fusion at order $\mathcal{O}(\alpha_s^4)$* , *JHEP* **08** (2012) 139, [[arXiv:1206.0157](#)].
- [67] T. Neumann and M. Wiesemann, *Finite top-mass effects in gluon-induced Higgs production with a jet-veto at NNLO*, *JHEP* **11** (2014) 150, [[arXiv:1408.6836](#)].
- [68] J. M. Campbell, R. K. Ellis, R. Frederix, P. Nason, C. Oleari, and C. Williams, *NLO Higgs Boson Production Plus One and Two Jets Using the POWHEG BOX, MadGraph4 and MCFM*, *JHEP* **07** (2012) 092, [[arXiv:1202.5475](#)].
- [69] K. Hamilton, P. Nason, C. Oleari, and G. Zanderighi, *Merging $H/W/Z + 0$ and 1 jet at NLO with no merging scale: a path to parton shower + NNLO matching*, *JHEP* **05** (2013) 082, [[arXiv:1212.4504](#)].
- [70] M. Buschmann, D. Goncalves, S. Kuttimalai, M. Schonherr, F. Krauss, and T. Plehn, *Mass Effects in the Higgs-Gluon Coupling: Boosted vs Off-Shell Production*, *JHEP* **02** (2015) 038, [[arXiv:1410.5806](#)].
- [71] R. Frederix, S. Frixione, E. Vryonidou, and M. Wiesemann, *Heavy-quark mass effects in Higgs plus jets production*, *JHEP* **08** (2016) 006, [[arXiv:1604.03017](#)].
- [72] N. Greiner, S. Höche, G. Luisoni, M. Schönerr, and J.-C. Winter, *Full mass dependence in Higgs boson production in association with jets at the LHC and FCC*, *JHEP* **01** (2017) 091, [[arXiv:1608.01195](#)].
- [73] F. Maltoni, E. Vryonidou, and M. Zaro, *Top-quark mass effects in double and triple Higgs production in gluon-gluon fusion at NLO*, *JHEP* **11** (2014) 079, [[arXiv:1408.6542](#)].
- [74] A. Gehrmann-De Ridder, T. Gehrmann, and E. W. N. Glover, *Antenna subtraction at NNLO*, *JHEP* **09** (2005) 056, [[hep-ph/0505111](#)].
- [75] A. Gehrmann-De Ridder, T. Gehrmann, and E. Glover, *Gluon-gluon antenna functions from Higgs boson decay*, *Phys. Lett. B* **612** (2005) 49–60, [[hep-ph/0502110](#)].
- [76] A. Daleo, T. Gehrmann, and D. Maitre, *Antenna subtraction with hadronic initial states*, *JHEP* **04** (2007) 016, [[hep-ph/0612257](#)].
- [77] A. Daleo, A. Gehrmann-De Ridder, T. Gehrmann, and G. Luisoni, *Antenna subtraction at NNLO with hadronic initial states: initial-final configurations*, *JHEP* **01** (2010) 118, [[arXiv:0912.0374](#)].
- [78] E. W. Nigel Glover and J. Pires, *Antenna subtraction for gluon scattering at NNLO*, *JHEP* **06** (2010) 096, [[arXiv:1003.2824](#)].
- [79] A. Gehrmann-De Ridder, E. W. N. Glover, and J. Pires, *Real-Virtual corrections for gluon scattering at NNLO*, *JHEP* **02** (2012) 141, [[arXiv:1112.3613](#)].

- [80] A. Gehrmann-De Ridder, T. Gehrmann, and M. Ritzmann, *Antenna subtraction at NNLO with hadronic initial states: double real initial-initial configurations*, *JHEP* **1210** (2012) 047, [[arXiv:1207.5779](#)].
- [81] A. Gehrmann-De Ridder, T. Gehrmann, E. W. N. Glover, and J. Pires, *Double Virtual corrections for gluon scattering at NNLO*, *JHEP* **02** (2013) 026, [[arXiv:1211.2710](#)].
- [82] J. Currie, E. Glover, and S. Wells, *Infrared Structure at NNLO Using Antenna Subtraction*, *JHEP* **04** (2013) 066, [[arXiv:1301.4693](#)].
- [83] F. Cascioli, P. Maierhofer, and S. Pozzorini, *Scattering Amplitudes with Open Loops*, *Phys. Rev. Lett.* **108** (2012) 111601, [[arXiv:1111.5206](#)].
- [84] F. Buccioni, S. Pozzorini, and M. Zoller, *On-the-fly reduction of open loops*, *Eur. Phys. J. C* **78** (2018), no. 1 70, [[arXiv:1710.11452](#)].
- [85] F. Buccioni, J.-N. Lang, J. M. Lindert, P. Maierhöfer, S. Pozzorini, H. Zhang, and M. F. Zoller, *OpenLoops 2*, *Eur. Phys. J. C* **79** (2019), no. 10 866, [[arXiv:1907.13071](#)].
- [86] J.-N. Lang et al, *OTTER: On-The-fly Tensor Reduction*, *In preparation*.
- [87] R. Frederix, S. Frixione, V. Hirschi, F. Maltoni, O. Mattelaer, P. Torrielli, E. Vryonidou, and M. Zaro, *Higgs pair production at the LHC with NLO and parton-shower effects*, *Phys. Lett. B* **732** (2014) 142–149, [[arXiv:1401.7340](#)].
- [88] S. Catani, *The Singular behavior of QCD amplitudes at two loop order*, *Phys. Lett. B* **427** (1998) 161–171, [[hep-ph/9802439](#)].
- [89] M. Grazzini, G. Heinrich, S. Jones, S. Kallweit, M. Kerner, J. M. Lindert, and J. Mazzitelli, *Higgs boson pair production at NNLO with top quark mass effects*, *JHEP* **05** (2018) 059, [[arXiv:1803.02463](#)].
- [90] A. Denner, S. Dittmaier, and L. Hofer, *COLLIER: a fortran-based Complex One-Loop Library in Extended Regularizations*, *Comput. Phys. Commun.* **212** (2017) 220–238, [[arXiv:1604.06792](#)].
- [91] A. van Hameren, *OneLoop: For the evaluation of one-loop scalar functions*, *Comput. Phys. Commun.* **182** (2011) 2427–2438, [[arXiv:1007.4716](#)].
- [92] A. von Manteuffel and C. Studerus, *Reduze 2 - Distributed Feynman Integral Reduction*, [[arXiv:1201.4330](#)].
- [93] Z. Li, J. Wang, Q.-S. Yan, and X. Zhao, *Efficient numerical evaluation of Feynman integrals*, *Chin. Phys. C* **40** (2016), no. 3 033103, [[arXiv:1508.02512](#)].
- [94] S. Borowka, G. Heinrich, S. Jahn, S. P. Jones, M. Kerner, and J. Schlenk, *A GPU compatible quasi-Monte Carlo integrator interfaced to pySecDec*, *Comput. Phys. Commun.* **240** (2019) 120–137, [[arXiv:1811.11720](#)].
- [95] J. Baglio, F. Campanario, S. Glaus, M. Mühlleitner, M. Spira, and J. Streicher, *Gluon fusion into Higgs pairs at NLO QCD and the top mass scheme*, *Eur. Phys. J. C* **79** (2019), no. 6 459, [[arXiv:1811.05692](#)].
- [96] J. Baglio, F. Campanario, S. Glaus, M. Mühlleitner, J. Ronca, M. Spira, and J. Streicher, *Higgs-Pair Production via Gluon Fusion at Hadron Colliders: NLO QCD Corrections*, *JHEP* **04** (2020) 181, [[arXiv:2003.03227](#)].
- [97] J. Baglio, F. Campanario, S. Glaus, M. Mühlleitner, J. Ronca, and M. Spira, *$gg \rightarrow HH$: Combined uncertainties*, *Phys. Rev. D* **103** (2021), no. 5 056002, [[arXiv:2008.11626](#)].
- [98] S. Amoroso et al., *Les Houches 2019: Physics at TeV Colliders: Standard Model Working Group Report*, in *11th Les Houches Workshop on Physics at TeV Colliders: PhysTeV Les Houches*, 3, 2020. [[arXiv:2003.01700](#)].

- [99] J. Butterworth et al., *PDF₄LHC recommendations for LHC Run II*, *J. Phys. G* **43** (2016) 023001, [[arXiv:1510.03865](#)].
- [100] M. Cacciari, G. P. Salam, and G. Soyez, *The anti- k_t jet clustering algorithm*, *JHEP* **04** (2008) 063, [[arXiv:0802.1189](#)].